



# Hydrolysis Stability of Bidentate Phosphites Utilized as Modifying Ligands in the Rh-Catalyzed *n*-Regioselective Hydroformylation of Olefins

Baoxin Zhang,<sup>\*,§</sup> Haijun Jiao,<sup>§</sup> Dirk Michalik,<sup>§,†</sup> Svenja Kloss,<sup>†</sup> Lisa Marie Deter,<sup>†</sup> Detlef Selent,<sup>§</sup> Anke Spannenberg,<sup>§</sup> Robert Franke,<sup>||,‡</sup> and Armin Börner<sup>\*,§,†</sup>

<sup>§</sup>Leibniz-Institut für Katalyse an der Universität Rostock e.V., Albert-Einstein-Str. 29a, D-18059 Rostock, Germany

<sup>†</sup>Institut für Chemie der Universität Rostock, Albert-Einstein-Str. 3, D-18059 Rostock, Germany

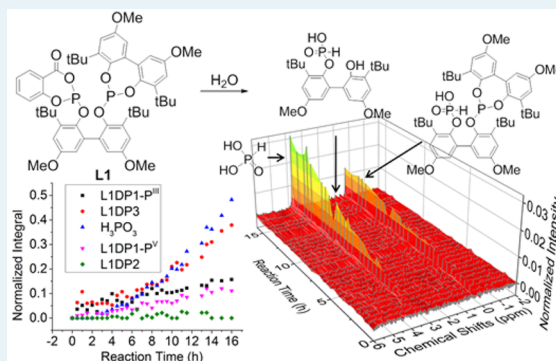
<sup>||</sup>Evonik Performance Materials GmbH, Paul-Baumann-Str. 1, D-45772 Marl, Germany

<sup>‡</sup>Lehrstuhl für Theoretische Chemie, Ruhr-Universität Bochum, D-44780 Bochum, Germany

## S Supporting Information

**ABSTRACT:** The stability of ligands and catalysts is an almost neglected issue in homogeneous catalysis, but it is crucial for successful application of this methodology in technical scale. We have studied the effect of water on phosphites, which are the most applied cocatalysts in the *n*-regioselective homogeneous Rh-catalyzed hydroformylation of olefins. The stability of the bidentate nonsymmetrical diphosphite L1, as well as its two monophosphite constituents L2 and L3, toward hydrolysis was investigated by means of in situ NMR spectroscopy under similar conditions as applied in industry. Hydrolysis pathways, intermediates, and kinetics were clarified. DFT calculations were used to support the experimentally found data. The acylphosphite unit L2, which reacts with water in an unselective manner, was proven to be much less stable than the phenolphosphite L3. The stability of the bidentate ligand L1 can be therefore mainly attributed to its phenolphosphite moiety. With an excess of water, the hydrolysis of L1 and L2 as well as their Rh-complexes is first-order with respect to the phosphite. Surprisingly, coordination to Rh significantly stabilizes the monodentate ligand L2, while in strong contrast, the bidentate ligand L1 decomposes faster in the Rh complex. NMR spectroscopy provided evidence for the existence of species from decomposition of phosphites, which can likewise coordinate as ligands to the metal. Electron-withdrawing groups in the periphery of the acylphosphite moiety decrease the stability of L1, whereas 3,5-disubstituted salicylic acid derivatives with bulky groups showed superior stability. These modifications of L1 also give rise to different catalytic performances in the *n*-regioselective hydroformylation of *n*-octenes and 2-pentene, from which the 3,5-di-*t*-butyl-substituted ligand offered a higher *n*-regioselectivity accompanied by a lowering of the reaction rate in comparison to the parent ligand L1.

**KEYWORDS:** homogeneous catalysis, phosphite, hydroformylation, rhodium, hydrolysis stability



## 1. INTRODUCTION

A catalyst accelerates the rate of chemical reactions by lowering of the energies of transition states by forming associates with the substrate. In the final step of the catalytic cycle, the catalyst is released from the product. In most textbooks, it is conceptually assumed that the catalyst is fully regenerated and therefore remains unchanged over the whole catalytic process. However, in practice, the highly reactive catalyst is frequently altered due to side reactions with other components in the reaction mixture (e.g., intermediates, products, solvents as well as impurities), which may lead to deviations from the expected catalytic activity and selectivity.<sup>1</sup>

Unlike in heterogeneously catalyzed processes, where the deactivated catalyst can be easily isolated and separated, any separation or concentration processes in homogeneous catalysis

may lead to further degradations of the relevant catalytically active or nonactive species causing ambiguous analytic results. Moreover, the low concentration of the catalyst under application conditions requires specific spectroscopic methods for analysis. Therefore, studies addressing the stability of homogeneous catalysts are very challenging and up to now quite rare.<sup>1,2</sup>

Of particular economic and academic importance is the *n*-regioselective hydroformylation of olefins.<sup>3</sup> It is worldwide one of the largest homogeneously catalyzed processes on an industrial scale. Aldehydes produced are valuable final products

**Received:** August 2, 2016

**Revised:** September 7, 2016

**Published:** September 12, 2016

in bulk and fine chemistry. They can be easily transformed into numerous other functionalized compounds like alcohols, esters, and amines. In comparison to conventionally applied cobalt catalyst,<sup>4</sup> the more recently developed rhodium-based systems modified with trivalent phosphorus ligands offer the advantage of running the reaction at much lower syngas pressure (1.8–6.0 MPa) and moderate temperatures (85–130 °C).<sup>5</sup>

An issue of enormous importance is the stability of the precious rhodium catalyst. In continuous approaches, its integrity has to be assured over several days, weeks, or even months. Decomposition of the original phosphorus ligand and loss of its ligating properties lower the concentration of the active catalyst. As a consequence, an alteration of the desired catalytic results takes place. Due to the loss of the organic ligand, “naked” rhodium reacts with CO to give nonselective, less active, and finally, entirely inactive rhodium carbonyl clusters. Also, in batch reactions, the reuse of the original catalyst is of great value due to its high cost.

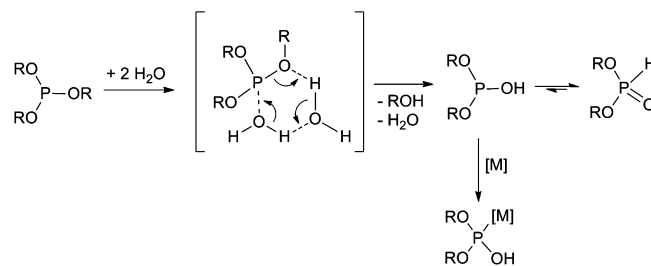
Decomposition pathways depend on the nature of the phosphorus ligands and reaction conditions applied. Phosphines are prone to oxidation and P–C bond activation, whereas phosphorus ligands with P–O bonds, especially phosphites, suffer solvolysis with water.<sup>7</sup> In technical hydroformylation conditions, water is continuously formed together with the so-called high-boilers due to the aldol condensation of the product aldehydes. Because phosphites generate more active catalysts for the *n*-regioselective hydroformylation of olefins than phosphines, they constitute one of the most utilized classes of ligands in this regard. Especially, bidentate diphosphites are regularly applied. With the assistance of such diphosphites, hundred thousands of tons aldehydes are produced annually. Therefore, their behaviors toward water are of crucial importance, especially for the design of more resistant ligands and for the proper choice of the reaction conditions (temperature, removal of water, etc.).<sup>8</sup> Besides, to mitigate the degradation of phosphites, usually proper stabilizers containing tertiary amines or epoxides, or the ion-exchange methods are applied in industry.<sup>9</sup>

The effect of water on phosphites, as well as on phosphinites and phosphonites, is due to the nucleophilic attack of P–O bonds. As a result, the alkoxy or aryloxy is substituted. Primarily, the product with trivalent phosphorus is stabilized as tetravalent oxide species by tautomerism.<sup>4</sup>

It was reported in the older literature that the hydrolysis of trialkylphosphites follows a first-order kinetics in phosphite and a second-order in water (Scheme 1).<sup>10</sup> Spectroscopic experiments with <sup>18</sup>O- and <sup>17</sup>O-labeled water and measurement of a strong isotope effect with D<sub>2</sub>O provided evidence that a P–O- and not a C–O-bond is cleaved and that the attack of water on phosphorus is the rate-determining step.<sup>11</sup>

Hydrolysis products of phosphites do not compellingly lose their complexation properties. Due the phosphinylidene tautomerization, the trivalent phosphorous acid diester is able to coordinate on metals. This property of H-phosphonates, also abbreviated as HASPOs (heteroatom-substituted phosphine oxides), stimulated several research groups to elucidate the relevant tautomeric equilibrium,<sup>12</sup> their coordination behavior to metals,<sup>13</sup> and catalytic properties of formed metal complexes.<sup>14,15</sup> Remarkably, already several years ago, van Leeuwen utilized a simple HASPO (HP(O)Ph<sub>2</sub>) in the platinum-catalyzed hydroformylation,<sup>16</sup> which clearly suggests that the catalytic impact of such degradation products should not be underestimated. With one exception concerned to the

**Scheme 1. Hydrolysis of the P–O-Bond and Competition between Formation of a Tetravalent Oxide Phosphorus Compound and Coordination of the Trivalent Species to a Metal<sup>a</sup>**



<sup>a</sup>We use in this article the classic form P=O double bond and P<sup>V</sup> denoting this kind of species only for the sake of expression convenience.<sup>6</sup>

asymmetric rhodium-catalyzed hydrogenation,<sup>17</sup> in all other instances, HASPOs were prepared prior to the catalytic process. However, the fact that HASPOs can be formed as a result of the decomposition of phosphites during the catalytic reaction has been seldom in the focus. Only recently, we got evidence that a HASPO, which has been formed during a hydroformylation process from a phosphite due to hydrolysis is able to affect the Rh-catalyzed hydroformylation.<sup>18</sup>

In order to get a complete picture about the decomposition pathways and the unusual catalytically active intermediates, we have initiated a detailed study using in situ NMR spectroscopic analysis and theoretical calculations. As an example of technical relevance, we have chosen the hybrid bidentate phosphite **L1** containing a mixed anhydride moiety (acylphosphite) and a biphenol phosphite moiety (phenolphosphite) (Figure 1).<sup>19</sup>

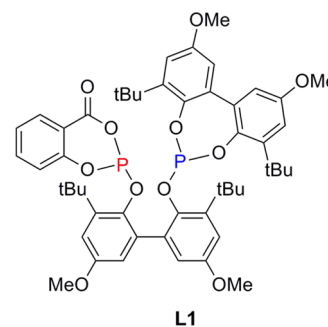


**Figure 1.** Bidentate hybrid diphosphite **L1**, in which the phosphite unit on the left-hand side is denoted as “acylphosphite” (red), and the part on the right-hand side is named herein “phenolphosphite” (blue).

Ligands based on this structure were proven to produce up to 69% *n*-nonanal in the Rh-catalyzed isomerizing hydroformylation of isomeric *n*-octenes containing only 3.3% terminal octene with turnover frequencies (TOF) up to 4700 h<sup>−1</sup>.

Due this excellent catalytic performance, their application in large-scale hydroformylations has been recommended. In this regard, the question of its hydrolysis stability is a crucial issue. With in situ <sup>1</sup>H, <sup>13</sup>C, and <sup>31</sup>P NMR spectroscopy and DFT calculations, the hydrolysis reactions of **L1** and each of its two phosphite components as well as their substructures were monitored qualitatively and quantitatively under conditions close to those as applied in industry. We found in our study that, in particular, in situ <sup>31</sup>P NMR spectroscopy is an ideal

method for studying degradation of such phosphites in a low concentration. Due to the 100% natural abundance of  $^{31}\text{P}$ , it has a high sensitivity to P-containing structures allowing a quantitative analysis. Moreover, usual hydrolysis products of phosphite are tetravalent phosphorus oxides, which have a polar P–O bond. Relevant signals appear near 0 ppm in the  $^{31}\text{P}$  NMR spectrum, whereas trivalent phosphites resonate between 120–150 ppm. Thus, a satisfying peak separation between product and reactant can be realized. This situation facilitates the interpretation of the spectra.

After these hydrolysis studies, the coordination modes of decomposition products to rhodium were evaluated. Subsequently, the hydrolysis resilience of phosphites as “free” ligands and in the Rh coordinated mode was compared. On the basis of these results, finally, a modification of the parent diphosphite has been carried out in order to improve its hydrolysis stability. Simultaneously, the effects of these modifications on the catalytic performance were evaluated.

## 2. EXPERIMENTAL SECTION

The hydrolysis experiment was performed in a 0.049 or 0.0245 M solution of the phosphite in 1,4-dioxane sealed in an NMR tube and quantitatively monitored by in situ  $^{31}\text{P}$  NMR spectroscopy. As an external reference a solution of tris(*n*-octyl)phosphine oxide (TOPO) dissolved in *p*-xylene- $d_{10}$  with a concentration of 0.259 M was sealed in a capillary and placed into the NMR tube together with the sample solution. The stability of TOPO toward hydrolysis and oxidation guarantees its constant amount and chemical properties during the whole experiment even at a high temperature. The sealed capillary makes sure that none of the components in the sample solution is interfered with by the reference. This setup created a separated reaction mixture, in which each species consumed and/or produced could be monitored qualitatively as well as quantitatively. The concentration of the external reference was regulated to give a comparable integral ratio between the phosphite and TOPO for the sake of accuracy. Integrals of the detected species normalized by that of TOPO can now be regarded as their concentrations in this isolated environment.

## 3. RESULTS AND DISCUSSION

**3.1. Hydrolysis of the Bidentate Hybrid Phosphite (L1).** Ligand L1 bears two different phosphite units. This electronically and sterically unsymmetric structure contains two alternative positions for the water attack. In order to assess the relative stability of the “left arm” and the “right arm” phosphite units in L1, the diphosphite was treated with 100 equiv of water at 120 °C.

In the beginning of the hydrolysis of L1, free salicylic acid and an intermediate phosphorous acid monoester (L1DP1) were detected by  $^1\text{H}$  NMR spectroscopy (left and middle spectra in Figure 2). L1DP1 exhibits signals of four nonequivalent *t*-Bu groups due to lack of  $C_s$  symmetry. In the  $^{31}\text{P}$  NMR spectrum, in addition to L1DP1 and the HASPO of L3 (structure discussed in section 3.6), here denoted as L1DP4, another compound (herein abbreviated as L1DP2) giving two signals in the *t*-Bu region was found and characterized by a singlet at 0.03 ppm. Further decomposition fragments of L1 such as free biphenol L1DP5 and phosphite phenol L1DP3 became subsequently discernible in the  $^1\text{H}$  NMR spectrum. At this stage of hydrolysis, the signal of phosphorous acid could also be attributed in the  $^{31}\text{P}$  NMR

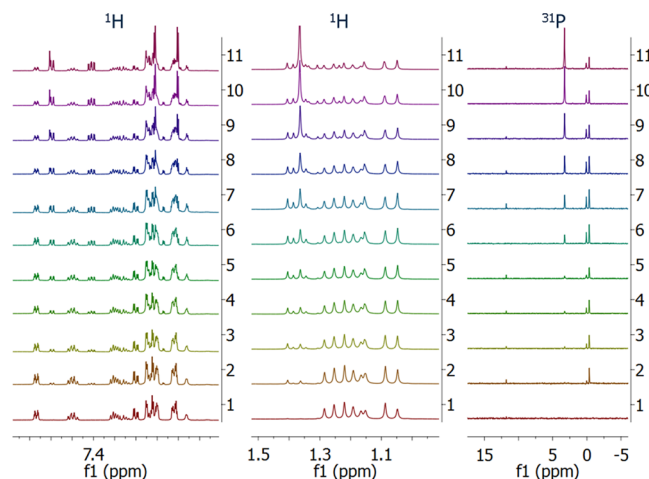


**Figure 2.** In situ  $^1\text{H}$  (left and middle, Ph and *t*Bu regions) and  $^{31}\text{P}$  (right,  $\text{P}^{\text{V}}$  region) NMR spectra of the hydrolysis of L1 with 100 equiv of water at 120 °C. Reaction time increased from below to above. The last spectrum was taken after 6.5 h of the hydrolysis.

spectrum. Corresponding P–H splittings of all phosphorous acid derivatives agree well in both  $^1\text{H}$  and  $^{31}\text{P}$  NMR spectra. Degradation to L1DP1 was additionally confirmed by in situ  $^{13}\text{C}$  NMR spectroscopy. After 5.5 h of heating with water, the only peaks of prominence could be attributed to salicylic acid and the substituted biphenol L1DP5.

Noticeably, in the  $^{31}\text{P}$  NMR spectra, no new signals appeared in the region of phosphites with a salicylic acid moiety. Also, no HASPO of the acylphosphite and/or its derivatives could be detected. An acylphosphite phenol structure has been proven to be unstable. Thus, the only possible phosphorous acid derivative derived from L1 with two nonequivalent *t*-Bu groups is a phosphorous acid monoester with the biphenol (L1DP2 in Scheme 2). From these observations, the hydrolysis pathway of L1 can be established. L1 is selectively hydrolyzed to L1DP1 in the first step. Hydrolysis of L1DP1 leads unselectively either to the phosphite phenol L1DP3 or to the monoester L1DP2 and the HASPO L1DP4. The latter is decomposed to L1DP2, which is in accord with the unsteadily low concentration profile of the HASPO found in the in situ  $^{31}\text{P}$  NMR spectra. As described previously, the phosphite phenol (L1DP3) is quite resistant toward hydrolysis.<sup>15</sup> It is accumulated in the product mixture. L1DP2 degrades finally to the free biphenol (L1DP5) and phosphorous acid. According to the proposed pathway, the amount of phosphorous acid should be equal to the sum of L1DP3 and L1DP5, which was verified by the quantitative analysis of the NMR spectra. The assignment of the signals of time-dependent  $^{31}\text{P}$  NMR spectra was achieved (Figure 3). Fitting concentration correlations of L1DP3/ $\text{H}_3\text{PO}_3$  and  $\text{P}^{\text{III}}/\text{P}^{\text{V}}$  of L1DP1 consisting with the proposed pathway could be extracted from concentration profiles of the products. The decay in concentration of L1 obeys first-order kinetics under the flooding condition, showing a half-life time of 24.49 h at 120 °C. A comparison of half-life times of L1 under different conditions can be found in the Supporting Information.

**3.2. Hydrolysis of Monoacylphosphite L2.** As evidenced above, the acylphosphite unit is more sensitive to the attack of water. In order to simplify the analysis of the highly complicated NMR spectra of the emerging hydrolysis intermediates, we investigated the hydrolysis of an isolated monophosphite structure derived from the structure of L1. The



Scheme 2. Hydrolysis Pathways of L1

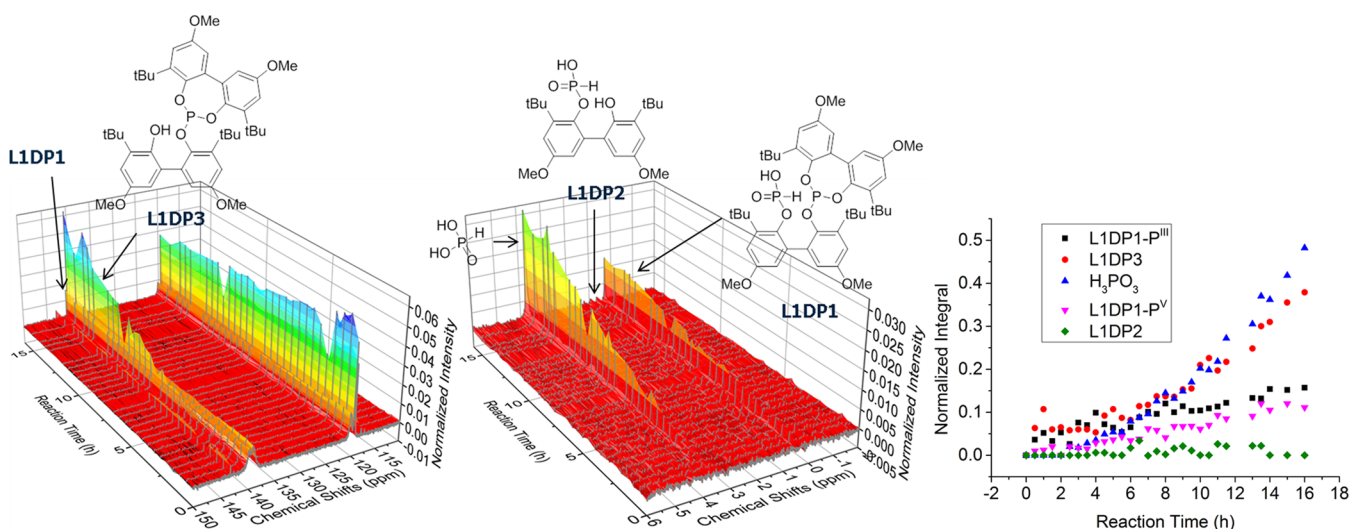
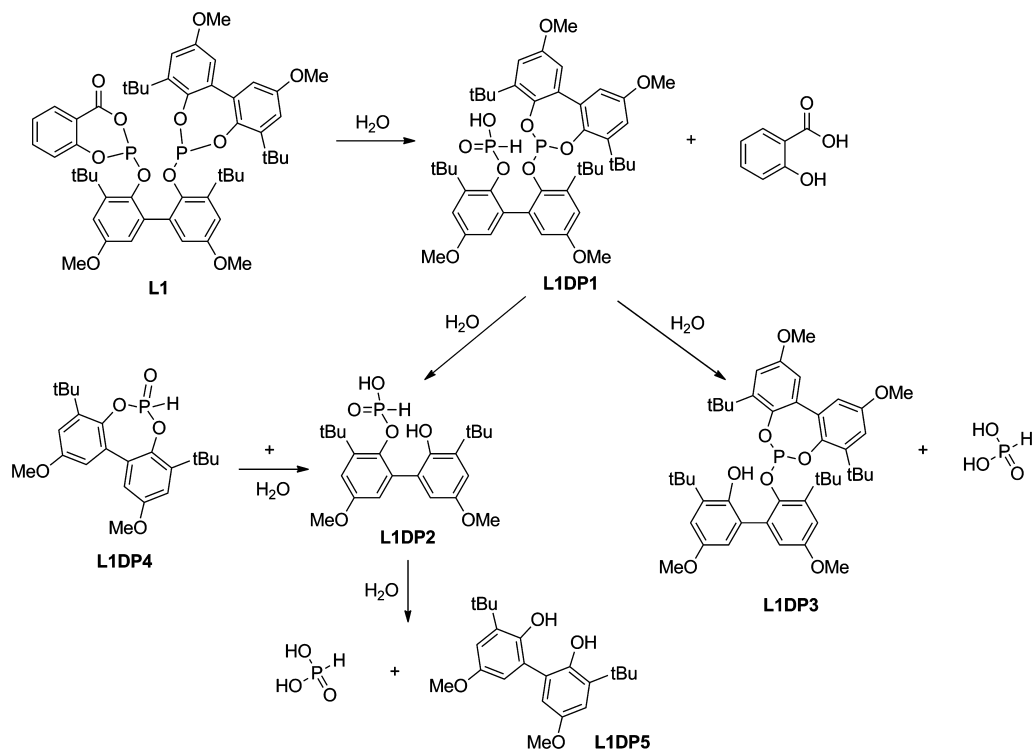


**Figure 3.** In situ <sup>31</sup>P NMR spectra of hydrolysis of L1 (100 equiv of water, 120 °C): phosphite (P<sup>III</sup>) region (left), tetraivalent oxide phosphorus (P<sup>V</sup>) region (middle) and concentration profiles of hydrolysis products of L1 (100 equiv of water, 120 °C) (right).

monoacylphosphite L2 as a model for the “left arm” of L1 consists of a six-membered cyclic mixed anhydride. It was prepared by the reaction of salicyl phosphorochloridite and 2-(*tert*-butyl)-4-methoxyphenol. Its molecular structure was solved with X-ray single crystal diffraction (Figure 4). The structure, in which three P–O bonds are of similar lengths, has a distorted trigonal pyramidal geometry about phosphorus with the lone electron pair pointing toward the apical direction.

We first studied the hydrolysis of L2 with a 10-fold amount of water (Figure 5). The concentration profile of the starting phosphite under this flooding condition follows a first-order kinetic with respect to L2, giving a half-life time of 16.5 h at room temperature. Two P-containing products from the degradation process were observed and characterized by

resonances at  $\delta = 2.6\text{--}3.6$  ppm ( $^1J_{\text{P,H}} = 700$  Hz) and  $\delta = 4.5\text{--}6.3$  ppm ( $^1J_{\text{P,H}} = 683$  Hz), respectively. Both resonances represent tetraivalent phosphorus oxide species whose normalized integrals along with the hydrolysis show that the latter is the predominant product. Both signals shifted downfield when the reaction progressed.<sup>20</sup>

For a more detailed understanding of the hydrolysis mechanism of L2, in turn, it was treated with only one equimolar amount of water. The reaction was again monitored by in situ NMR spectroscopy. Under the same conditions, four new sets of signals appeared in the time-dependent quantitative <sup>31</sup>P NMR spectra (Figure 6). All resonances are located in the region typical for P<sup>V</sup> compounds. According to its concen-

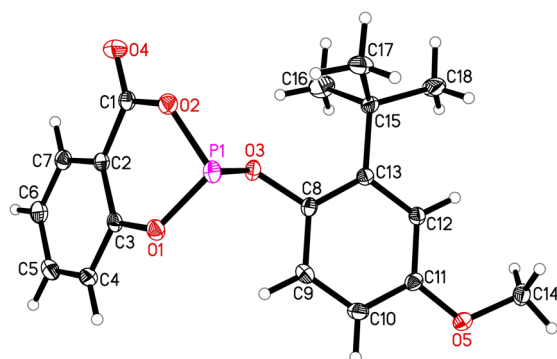


**Figure 4.** Molecular structure of **L2** (thermal ellipsoids at the 30% probability level). Selected bond lengths [Å] and angles [°]: P1–O1 1.631(1), P1–O2 1.638(1), P1–O3 1.632(1), O1–P1–O3 102.09(5), O2–P1–O3 94.65(5), O1–P1–O2 99.93(5).

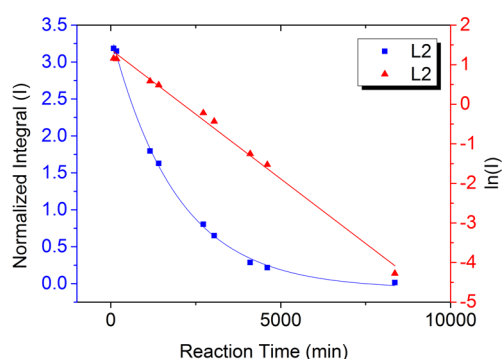


**Figure 5.** Concentration profile during the hydrolysis of **L2** with 10 equiv of water at room temperature.

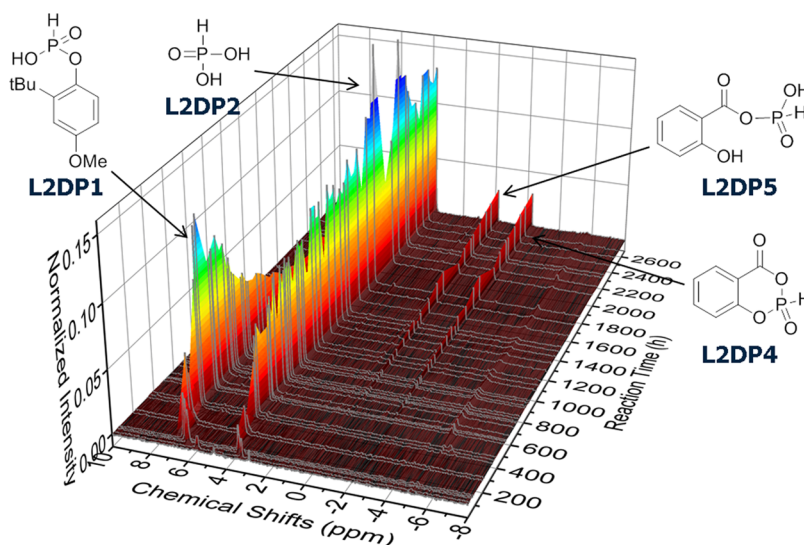
tration profile, the concentration of the product at  $\delta = 6.5\text{--}7.1$  ppm ( $^1J_{\text{P,H}} = 689$  Hz) increased at the beginning. This period is followed by a decrease of the concentration toward the end. The other three species showed steadily increasing concentration profiles. One signal (at  $\delta = 3.7$  ppm,  $^1J_{\text{P,H}} = 700$  Hz) even shows a high formation rate. In comparison to the hydrolysis experiment with the 10-fold amount of water, the trial with a phosphite/water ratio of 1:1 led to two new species

with constantly low concentration profile, besides the previously described main products.

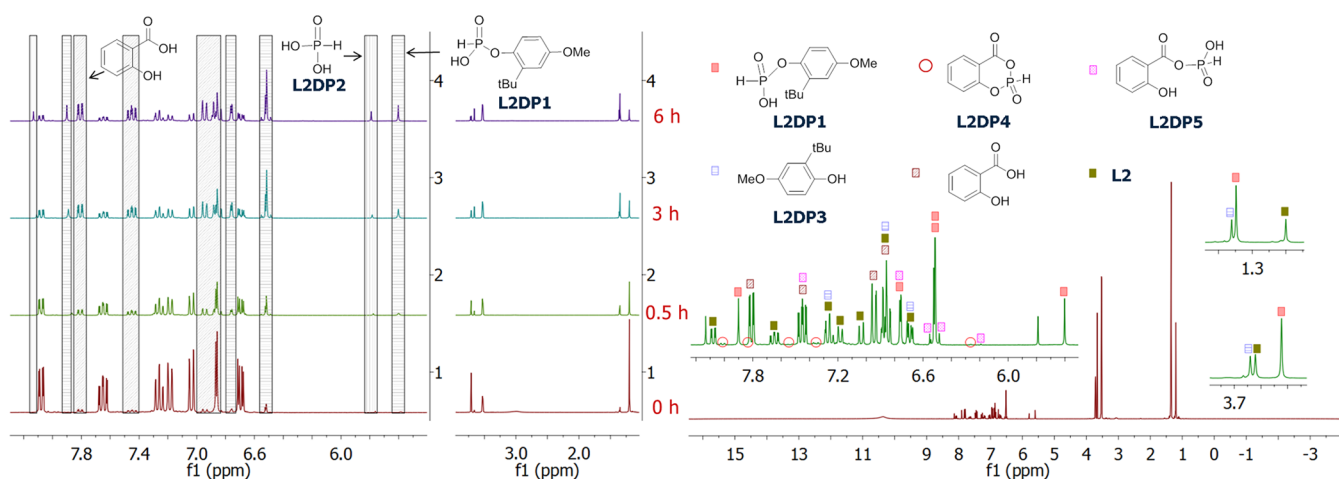
Notably, both hydrolysis experiments did not afford compounds characterized by  $^{31}\text{P}$  NMR peaks in the region typical for trivalent phosphorus.

The assignment of each product was confirmed by  $^1\text{H}$  NMR spectroscopy. To accelerate the reaction, the hydrolysis was performed at  $90^\circ\text{C}$ . The complete assignment of the signals in the  $^1\text{H}$  NMR spectrum of the reaction mixture was based on the chemical shifts, coupling constants, intensities of the  $^1\text{H}$  and  $^{13}\text{C}$  signals, and the results of two-dimensional NMR spectra ( $^1\text{H}, ^1\text{H}$  COSY,  $^1\text{H}, ^1\text{H}$  NOESY,  $^1\text{H}, ^{13}\text{C}$  HSQC,  $^1\text{H}, ^{13}\text{C}$  HMBC). **Figure 7** and **8** show an example describing the emerged components after a hydrolysis experiment at  $90^\circ\text{C}$  for 6 h. We found four P–H signals. Their coupling constants correspond well to those measured in the time-dependent  $^{31}\text{P}$  NMR spectra. The same holds for the relation of their integrals. This finding allows an interpretation of the four  $^{31}\text{P}$  NMR peaks for products (**Figure 6**). Several overlapped signals could be identified by integration, which remain true for every measured spectrum, referenced by the MeO- and *t*-Bu-signals of higher resolution. An interesting feature of the tetravalent phosphorus species found in the products is that their P–H chemical shifts as well as P–H coupling constants vary depending on the pH value and water amount of the solution. This observation was made in both the  $^1\text{H}$  and  $^{31}\text{P}$  NMR spectra.

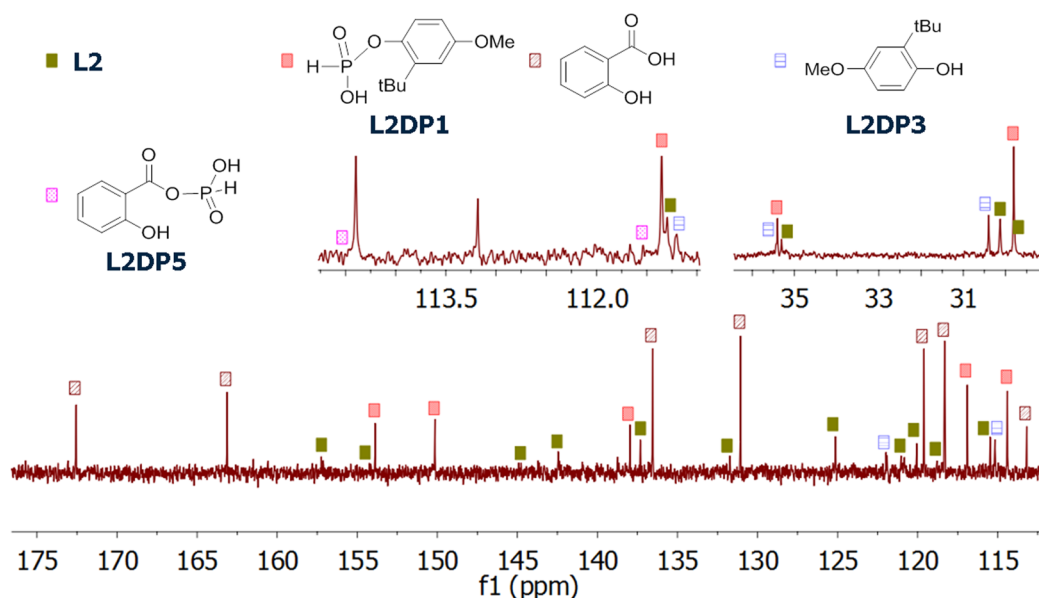
As illustrated in **Figure 7**, two new species bearing MeO- and *t*-butyl-groups became observable after 0.5 h of reaction. One compound contains a proton directly bound to phosphorus appearing at  $\delta = 6.8$  ppm with a large P–H coupling constant of 690 Hz. This P–H coupling constant is consistent with that observed in the  $^{31}\text{P}$  NMR spectra observed at  $\delta = 6.5\text{--}7.1$  ppm. It characterizes **L2DP1**. We also observed signals of the four aryl protons of salicylic acid which is released from the starting phosphite. Another P–H signal, found at  $\delta = 7.0$  ppm ( $^1J_{\text{P,H}} = 703$  Hz), can be unambiguously assigned to phosphorous acid corresponding to the signal at  $\delta = 3.7$  ppm ( $^1J_{\text{P,H}} = 700$  Hz) in the  $^{31}\text{P}$  NMR spectra and belongs to phosphorous acid (**L2DP2**). The integral ratios of **L2DP1** and **L2DP2** in the  $^1\text{H}$  and  $^{31}\text{P}$  NMR spectra were in nice agreement. After 6 h of reaction time, signals of sets of three aryl protons became



**Figure 6.** Hydrolysis of **L2** (with 1 equiv of water, at room temperature) monitored with in situ  $^{31}\text{P}$  NMR spectroscopy ( $\text{P}^{\text{V}}$  region).



**Figure 7.** Left: selected in situ  $^1\text{H}$  NMR spectra for hydrolysis of **L2** with 1 equiv of water at  $90^\circ\text{C}$  (low-field and high-field regions). Right: assignment of the  $^1\text{H}$  NMR spectrum of the reaction solution after hydrolysis with 1 equiv of water at  $90^\circ\text{C}$  for 6 h.

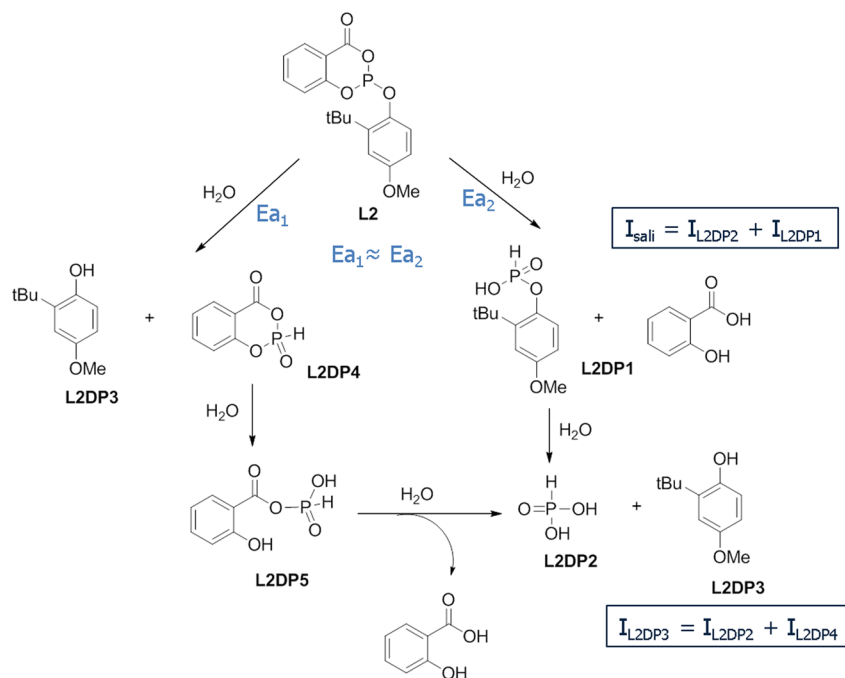


**Figure 8.**  $^{13}\text{C}$  NMR spectrum with assignment of reaction mixture of hydrolysis of **L2** ( $90^\circ\text{C}$ , 1 equiv of water, after 6 h).

visible characterizing two new aryl compounds with MeO- and *t*-Bu-groups. These signals were overlapped by peaks of **L2** and salicylic acid. One set of the new signals belongs to 4-methoxy-3-*t*-butyl-phenol (**L2DP3**) that arises from the hydrolysis of the exocyclic P–O bond of **L2**. The other product is a HASPO based on the six-membered ring with salicylic acid backbone. The four aryl proton peaks of the HASPO (**L2DP4**) were found as well although their intensity was low. The  $^1\text{H}$  chemical shifts of **L2DP4** were confirmed by comparison with the spectrum of the pure HASPO prepared in parallel by us. It displays a  $^{31}\text{P}$  resonance at  $\delta = -2.3$  ppm ( $^1J_{\text{P,H}} = 778$  Hz) which agrees well with the signal ( $\delta = -2.3$  ppm,  $^1J_{\text{P,H}} = 772$  Hz) detected in the hydrolysis experiment.

To summarize the in situ NMR investigations of the hydrolysis of **L2**, the following facts can be concluded: (a) at the beginning of hydrolysis signals of salicylic acid and phosphorous acid were observed accompanied by two species bearing a phenol moiety; (b) one of these new species has been identified as 4-methoxy-3-*t*-butyl-phenol (**L2DP3**) arising from the cleavage of the exocyclic P–O bond of **L2**; (c) signals of a

HASPO with a six-membered ring were likewise detected at the beginning of the hydrolysis; (d) by integral analysis, it was proven that the amount of salicylic acid was constantly equivalent to phosphorous acid and a new species formed. Also, the amount of the substituted phenol **L2DP3** was always equal to the sum of phosphorous acid and HASPO. Considering these observations with regard to the structure of **L2**, the only possible structure left bearing an anisole unit resulting from hydrolysis of **L2** is a phosphorous acid monoester, which will be herein denoted as **L2DP1**. It is released due to cleavage of the two endocyclic P–O bonds of the acylphosphite. The other product is salicylic acid. Taking in mind that the phenol **L2DP3** was already observed at the beginning of the hydrolysis together with the HASPO and that both compounds remained in a low concentration profile, the full hydrolysis pathways of **L2** can be described as illustrated in Scheme 3. Most intermediates of the decomposition are observable on the NMR time scale. In the presence of equimolar amounts of water, the hydrolysis of the mono-acylphosphite proceeds in an unselective manner. Either both

Scheme 3. Proposed Hydrolysis Pathways of L2<sup>a</sup>

<sup>a</sup>“I” means the normalized integral area.

endocyclic P–O bonds are cleaved simultaneously yielding the phosphorous acid monoester or the exocyclic P–O bond is broken giving rise to the HASPO L2DP4. These phosphorous acid mono- and diesters are prone to further degradation. Especially, L2DP4 immediately undergoes hydrolysis via L2DP5 to give phosphorous acid. Therefore, two stoichiometric relations shown in Scheme 3 can be deduced from these pathways, which are exactly in accordance with the experimental findings.

We were able to grow crystals from the hydrolysis product L2DP4. Its crystal structure is depicted in Figure 9. The

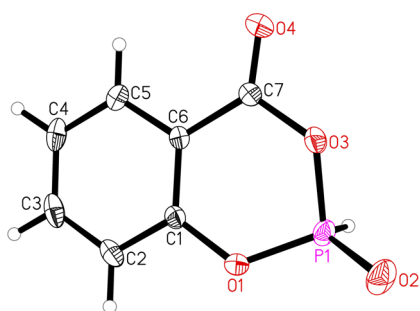


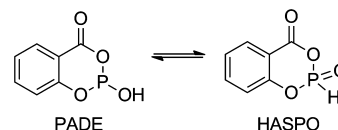
**Figure 9.** Molecular structure of L2DP4 (thermal ellipsoids at the 30% probability level). Selected bond lengths [Å] and angles [°]: P1–O1 1.575(2), P1–O2 1.456(2), P1–O3 1.585(2), O1–P1–O2 113.2(1), O2–P1–O3 112.1(1), O1–P1–O3 104.36(8).

relatively short bond P1–O2 (1.456 Å) suggests that the phosphorus atom is in the tetravalent state. Thus, in solid state, the molecule exists as HASPO isomer like that found in solution by NMR. In the <sup>31</sup>P NMR spectrum it resonates at –3.4 ppm (<sup>1</sup>J<sub>P,H</sub> = 760 Hz) in CD<sub>2</sub>Cl<sub>2</sub> and –2.3 ppm (<sup>1</sup>J<sub>P,H</sub> = 778 Hz) in our hydrolysis environment.

**3.3. DFT Calculations of the Hydrolysis of L2.** The question “Which P–O bond in L2 is most fragile against

water?” can be predicted by means of DFT calculations by comparing the free energy for each hydrolysis pathway. Scheme 4 illustrates the thermodynamic stability of all the possible

**Scheme 4. Tautomeric Equilibrium of L2DP4**

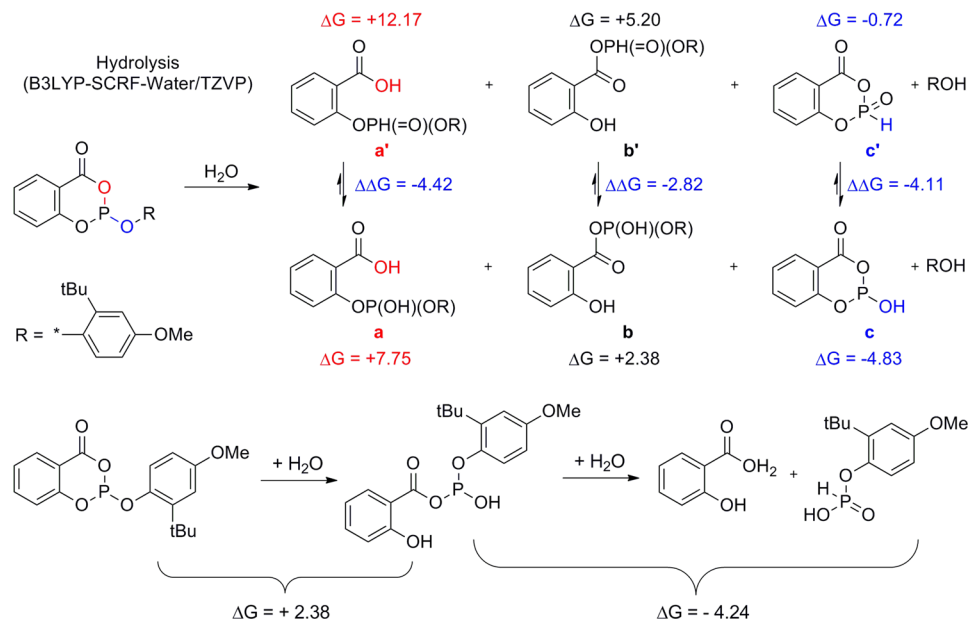


hydrolysis products of L2. For simplicity, water was chosen as solvent. The computed results give evidence that the exocyclic P–O bond is less stable. Therefore, it should be preferentially cleaved, followed by the cyclic ester bond. The anhydride P–O bond is the most stable one. Among the three pathways, only the cleavage of the exocyclic P–O bond is thermodynamically favored, giving rise to the corresponding HASPO, which could be in equilibrium with the corresponding phosphorous acid diester, here abbreviated as PADE (Scheme 5).

A controversial result to the experimental findings is the calculated result that the PADE isomer is thermodynamically more favored. It should be therefore predominant in the equilibrium with the HASPO isomer. It holds also for products from the second hydrolysis step. Due to the calculations, breakage of one of the P–O bonds in PADE is not favored, which would finally lead to phosphorous acid and salicylic acid. Another thermodynamically favored product is the phosphorous acid monoester L2DP1. Together with the six-membered cyclic HASPO/PADE and phosphorous acid, these three P-containing products are the only energetically preferred compounds emerging from the hydrolysis.

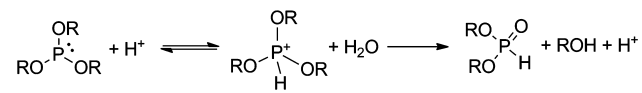
Concerning the experimental observations shown in Figure 6, that L2DP1 was the predominant product at the beginning of hydrolysis, and we conclude that the liberation of salicylic acid should be kinetically controlled.



Scheme 5. Changes of Gibbs Free Energy ( $\Delta G$ , kcal/mol) for Cleavage of Every P–O Bond in L2

It was found that the tautomeric equilibrium of the cyclic products could be reversed by a change of the chemical environment. For example, our calculation showed that in the 7-membered phenolphosphite unit **L1DP4** the equilibrium was shifted from the PADE to the HASPO isomer in an aqueous solution. Nevertheless, in gas phase, the PADE isomer was calculated to be more stable. Another explanation of the disparate results obtained by theoretical and experimental investigations could be the fact that the calculations refer to the hydrolysis in neutral conditions. However, it should be considered that in the experiment protons were increasingly generated from salicylic acid and phosphorous acid during progressing degradation process. We assume that the presence of protons leads to an alteration of the hydrolysis and favors simultaneously the tetravalent oxide isomer (Scheme 6).<sup>21</sup> By lowering

Scheme 6. Possible Hydrolysis Mechanism of Phosphite in the Presence of Protons



the energy barrier, it leads the reaction preferentially to the direction of the HASPO isomer. Thus, HASPO **L2DP4** and its decomposition intermediate **L2DP5** cannot be detected until a late stage of the hydrolysis, as recorded in Figure 5. The figure depicts an autocatalysis process triggered by progressively generated protons. It seems that protons have a strong impact not only on the PADE/HASPO equilibrium but also on the stability of these intermediates. Although **L2DP4** was continuously formed, its concentration was still kept constant at a low level in comparison to **L2DP1**. This observation can be rationalized by the fast subsequent hydrolysis of **L2DP4** via **L2DP5** to phosphorous acid (Scheme 3).

From calculated bond lengths, both the cyclic P–O bonds of **L2** become weaker after opening of the ring structure. As a consequence, the anhydride bond is weakened as expected and becomes less stable than the ester bond. In contrast, the

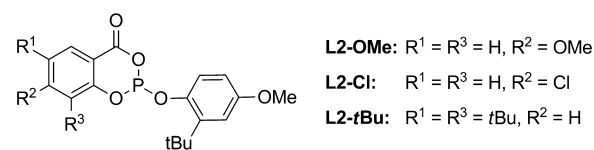
anhydride bond is more stable than the ester in the cyclic PADE-isomer (see results in Supporting Information).

Obviously, the intracyclic P–O bonds of the PADE isomer of **L2** get an extra stabilization by the almost planar six-membered ring and the anellation with the aryl ring. An electron-donating MeO-group in *p*-position to the acyl group of **L2** does not exert a significant stabilizing effect on the stability toward hydrolysis, which is in agreement with the experimental finding (vide infra). When it is replaced by the electron-withdrawing Cl-group, all three P–O bonds are activated.

**3.4. Stabilization Effects by Substituents.** In order to study the effect of substituents on the hydrolysis stability of the phosphite, a MeO- or *t*Bu-group was incorporated in the parent structure. Alternatively, as an electron-withdrawing substituent, Cl was chosen.

The influences of these substituents in the periphery of salicylic acid (Chart 1) on the hydrolysis stability in comparison

Chart 1. Derivatives of L2



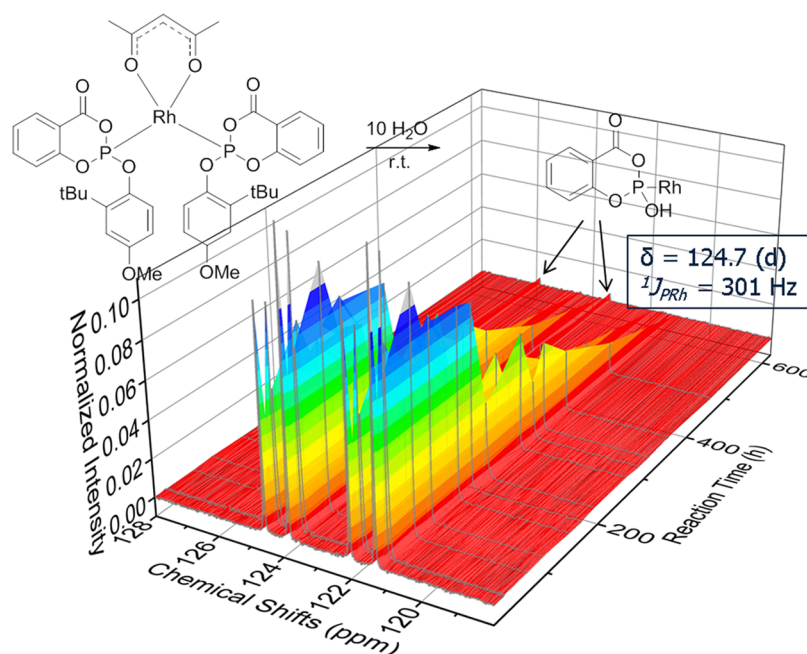
to **L2** are summarized in Table 1. Under the conditions detailed above, it can be concluded that the electron-donating MeO-group in the para position to the acyl moiety marginally improves the stability of the phosphite toward water. In

Table 1. Hydrolysis<sup>a</sup> of L2 and Its Derivatives

derivative	<i>t</i> 1/2 (h)
<b>L2</b>	17.8
<b>L2-OMe</b>	21.8
<b>L2-<i>t</i>Bu</b>	144.4
<b>L2-Cl</b>	after 1 h, only 58.7% of ligand left

<sup>a</sup>[L] = 0.049 M, 10 equiv of water, room temperature.





**Figure 10.** In situ  $^{31}\text{P}$  NMR spectra of hydrolysis of **RhL2** with 10 equiv of water at room temperature (phosphite region).

contrast, the electron-withdrawing Cl group in the same position destabilizes **L2** significantly. A clear improvement of hydrolysis resistance has been realized by application of the corresponding 3,5-di-*t*-butyl substituted salicylic acid derivative.

**3.5. Hydrolysis of L2 in Rh-Complex (RhL2).** Treatment of racemic **L2** with  $\text{Rh}(\text{CO})_2(\text{acac})$  in a molar ratio of 2:1 in toluene led to the complex  $\text{Rh}(\text{L2})_2(\text{acac})$  (**RhL2**). The  $^{31}\text{P}$  NMR spectrum of the complex displayed two sets of doublets centered at 122.0 and 122.4 ppm with couplings  $J_{\text{P,Rh}} = 305$  and 307 Hz, as expected for a mixture consisting of the *meso* isomer and the *R,R*- and *S,S*-enantiomers.

The time-dependent in situ  $^{31}\text{P}$  NMR spectra of the hydrolysis of **RhL2** at room temperature in the presence of 10-fold amount of water are depicted in Figure 10. The figure illustrates that besides the phosphite peaks of decreasing intensity, there is a new set of doublets appearing at  $\delta = 124.7$  ppm with a splitting of 301 Hz. Considering its typical chemical shift and coupling constant, the doublet can be attributed to the PADE of **L2** that has been coordinated to Rh. This observation gives proof that the degradation product of the monophosphite is able to coordinate to the metal. Simultaneously, the coordination retains the PADE form in equilibrium with its corresponding HASPO. Meanwhile, a very broad signal appeared around  $\delta = 80$  ppm. It might stem from a trivalent form of **L2DP1** with strong molecular dynamics. A new signal at  $\delta = 1.1$  ppm without P–H splitting was found additionally; however, its origin is still unclear. A resonance assigned to phosphorous acid could also be observed when the reaction was carried out at 90 °C for 5 h. The change of the concentration of the phosphite indicates that the hydrolysis obeys a first-order kinetic with respect to **L2**. The half-life time is 173 h, which is much longer than the half-time observed in the hydrolysis of the “free” ligand. This result gives clear evidence that coordination of the monodentate ligand to Rh stabilizes it toward hydrolysis. This stabilizing effect is manifested in the crystal structure of **RhL2** (Figure 11) by a shortening of two of the three P–O bonds of **L2** in comparison to the uncoordinated phosphite **L2**.

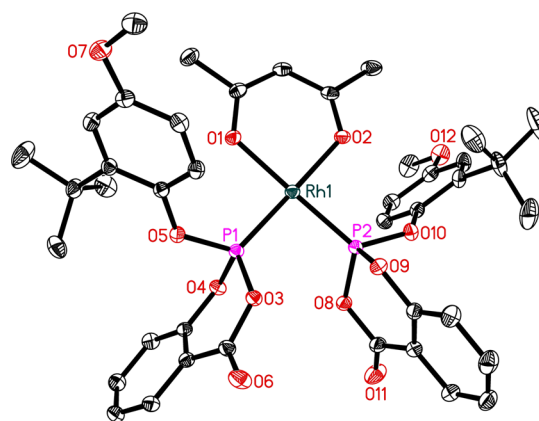
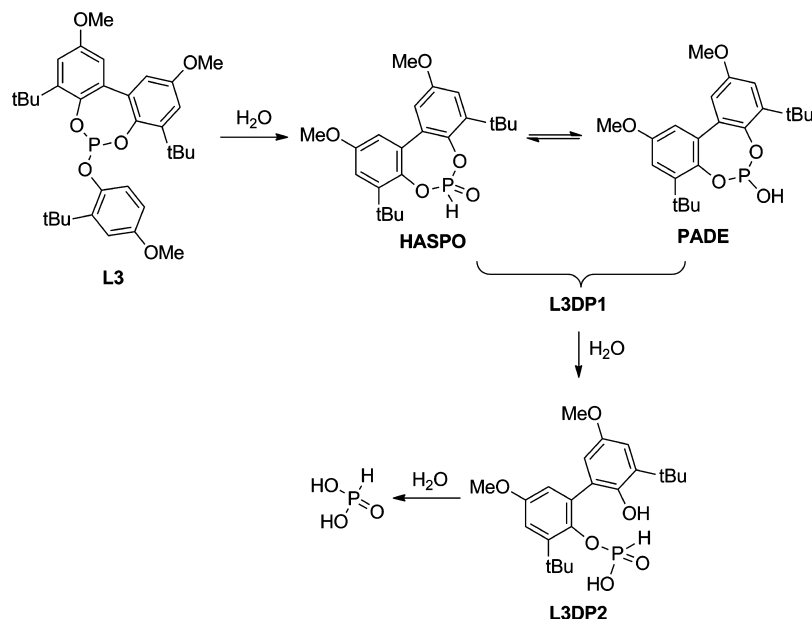


**Figure 11.** Molecular structure of **RhL2** (thermal ellipsoids at the 30% probability level; hydrogen atoms have been omitted for clarity). Selected bond lengths [Å] and angles [°]: P1–O3 1.632(1), P1–O4 1.614(1), P1–O5 1.594(1), P2–O8 1.633(1), P2–O9 1.607(1), P2–O10 1.601(1), Rh1–P1 2.1335(4), Rh1–P2 2.1322(4), O3–P1–O4 100.16(6), O4–P1–O5 97.14(6), O3–P1–O5 101.78(6), O8–P2–O9 100.85(6), O9–P2–O10 96.76(6), O8–P2–O10 102.02(6).

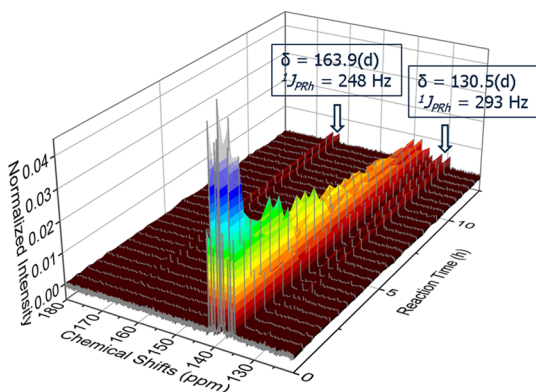
**3.6. Hydrolysis of the “Right Arm” of L1.** The “right arm” of **L1** is represented by the model phosphite **L3** (Scheme 7). The corresponding hydrolysis product **L3DP1** has been prepared and structurally analyzed previously in our group.<sup>18</sup> In its PADE-isomer this degradation product was able to act as a modifying ligand in the rhodium-catalyzed hydroformylation. The superior stabilizing effect of the biphenol in contrast to salicylic acid is demonstrated by comparing stabilities of the corresponding monophosphites (i.e., the acylphosphite **L2** and the phenolphosphite **L3**). Much higher resistance toward hydrolysis of the latter has been found. The phosphite remained almost intact in the presence of 10 equiv of water at 90 °C. In total, three products were detected by in situ  $^{31}\text{P}$  NMR spectroscopy, which were assigned to the HASPO of **L3** (**L3DP1**), a biphenol phosphorous acid monoester (**L3DP2**), and phosphorous acid, respectively (Scheme 7). According to

Scheme 7. Hydrolysis Pathway of L3



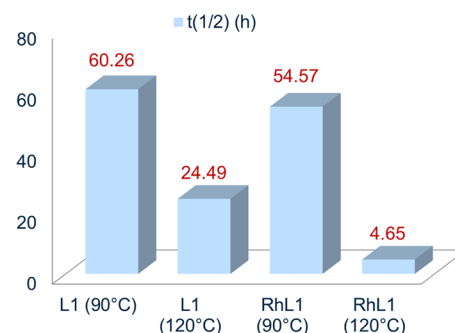
this result, the hydrolysis pathway of L3 can be unambiguously revealed. Unlike L2 its exocyclic P–O bond is first cleaved selectively followed by cleavage of one of the P–O bonds in the HASPO. A clear autocatalysis process can be concluded from the concentration profile of the components of the hydrolysis of L3. As the amount of  $\text{H}_3\text{PO}_3$  increased, the decomposition of the phosphite was dramatically accelerated (see results in Supporting Information)

**3.7. Hydrolysis of Rh-Complex of L1 (RhL1).** Rh(acac)-(L1) was hydrolyzed under the same conditions as employed for L1 (Figure 12). Surprisingly, the bidentate diphosphite was



**Figure 12.** In situ  $^{31}\text{P}$  NMR spectra of hydrolysis of RhL1 (100 equiv of water, 120 °C), where two new formed doublets appear in  $\text{P}^{\text{III}}$  region.

decomposed faster after coordination to the metal. As shown in Figure 13, a decrease of the half-life time of L1 was apparent, especially for the trial at 120 °C, where the destabilizing effect of Rh is remarkable. This finding is in strong contrast to that what has been observed for the monophosphite L2. Irrespective of this observation, a similar degradation pattern for the hydrolysis of both ligands was found. The in situ  $^{31}\text{P}$  NMR spectra showed a doublet signal ( $\delta = 130.5$  ppm) with a splitting of 293 Hz appearing in the phosphite region as well, together with another doublet at 163.9 ppm with a splitting of

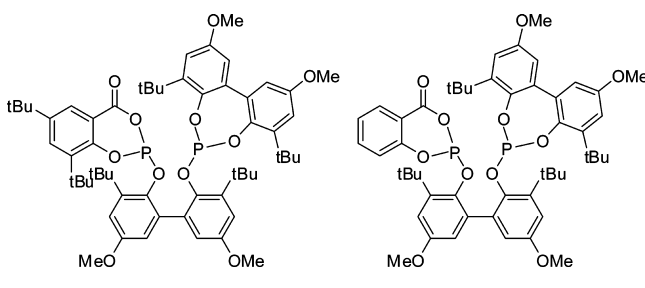


**Figure 13.** Comparison of half-life times of L1 and RhL1 at different hydrolysis temperatures.

248 Hz. With respect to the observations with RhL2, these signals can be clearly attributed to the hydrolysis products which coordinate to Rh after  $\text{P}^{\text{V}}$  to  $\text{P}^{\text{III}}$  tautomerization (e.g., HASPOs of L2 and L3). Unfortunately, under our conditions, no species having a P–H bond could be detected. Only a singlet at 0.6 ppm in the  $^{31}\text{P}$  NMR spectrum was observed.

**3.8. Optimization of the Structure of L1: L4.** As found above, an *ortho* placed *tert*-butyl group in the acylphosphite structure has a stabilizing effect on the hydrolysis resistance of the isolated “left” part of the bidentate ligand. In order to prove if this conclusion is also valid for the corresponding bidentate ligand, we synthesized ligand L4. As demonstrated in Table 2, the *tert*-butyl decorated diphosphite showed a superior stability in comparison to L1 at different temperatures. Notably, the stabilizing effect became more significant when the temperature was increased from 90 to 120 °C, which is especially important for the conditions of technical application.

**3.9. Hydroformylation of *n*-Octene and 2-Pentene: A Comparison of L1 and L4.** In order to elucidate which consequences arise from the application of a more stable ligand on the catalytic performance, we compared L1 and L4 in the hydroformylation of *n*-octenes and 2-pentene, respectively. Results are listed in Table 3 and Table 4. Interestingly, the results are dependent on the substrate used. L1 induced higher yields of aldehydes than L4 in the hydroformylation of *n*-

Table 2. Hydrolysis<sup>a</sup> of L1 and L4


derivative	$t_{1/2}/90\text{ }^{\circ}\text{C}$ (h)	$t_{1/2}/120\text{ }^{\circ}\text{C}$ (h)
L1	60.3	24.5
L4	91.2	45.6

<sup>a</sup>[L] = 0.0245 M, 100 equiv water.Table 3. Hydroformylation<sup>a</sup> of *n*-Octenes<sup>b</sup>

entry	ligand	Rh/L/ <i>n</i> -octenes	aldehydes <sup>c</sup> (%)	<i>n</i> -selectivity (%)	$k_{\text{obs}}$ <sup>d</sup> (min <sup>-1</sup> )
1	L1	1:5:2168	98	60.8	0.13363
2	L4	1:5:2131	88	70.7	0.06568

<sup>a</sup>[Rh] =  $0.77 \times 10^{-3}$  mol/L;  $T = 120\text{ }^{\circ}\text{C}$ ,  $p = 20$  bar total,  $t = 4$  h, solvent propylene carbonate. <sup>b</sup>3.3% 1-octene, 48.4% *Z*/*E*-2-octene, 29.2% *Z*/*E*-3-octene, 16.4% *Z*/*E*-4-octene, 2.1% skeletal C8-olefinic isomers, 0.6% *n*-octane. <sup>c</sup>Determined by GC with toluene as internal standard. <sup>d</sup>Pseudo-first-order rate constant derived from exponential curve fitting of gas consumption versus time.

Table 4. Hydroformylation<sup>a</sup> of 2-Pentene

entry	ligand	Rh/L/2-pentene	aldehydes <sup>b</sup> (%)	<i>n</i> -selectivity <sup>c</sup> (%)	$k_{\text{obs}}$ <sup>d</sup> (min <sup>-1</sup> )
1	L1	1:5:666	100	71.4	0.1769
2	L4	1:5:645	100	81.4	0.0456

<sup>a</sup>[Rh] =  $1.07 \times 10^{-3}$  mol/L;  $T = 120\text{ }^{\circ}\text{C}$ ,  $p = 20$  bar total,  $t = 1.5$  h, solvent propylene carbonate. <sup>b</sup>Determined by GC with toluene as internal standard. <sup>c</sup>Share of *n*-hexanal among aldehydes formed. <sup>d</sup>Pseudo-first-order rate constant derived from exponential curve fitting of gas consumption versus time.

octenes. Notably, the selectivity toward the formation of the desired *n*-aldehyde is superior in comparison with the less decorated ligand.

A similar result was obtained when 2-pentene was submitted to the reaction. The *tert*-butyl-decorated ligand L4 produced a less active but more selective catalyst in comparison to the parent ligand L1.

#### 4. CONCLUSIONS

The complete hydrolysis pathway of the bidentate hybrid diposphite L1 was clarified. The diposphite is of interest for the industrial application in the rhodium-catalyzed hydroformylation of olefins. In situ NMR spectroscopy gave evidence that salicylic acid is first released from the structure of L1. The resulting phosphorous acid monoester L1DP1 undergoes hydrolysis unselectively. By comparing the stability of the two monophosphite units in L1, it can be concluded that the “right arm” of the ligand is stabilized by its phenolphosphite moiety. In contrast, the acylphosphite L2 is quite sensitive toward water. Hydrolysis of L2 proceeds unselective and gives salicylic acid and phosphorous acid as main final products. The spectroscopic results were supported by DFT calculations.

Both degradations of L1 and L2 follow first-order kinetics with respect to the phosphite with an excessive amount of water.

Salicylic acid decorated with sterically demanding *t*-butyl groups in 3- and 5-position gives a ligand (L4) of much higher hydrolysis stability compared with unsubstituted L1. This is in line with the fact that the overwhelming amount of phosphites suggested as ligands in rhodium-catalyzed hydroformylation bear *t*-butyl groups in *ortho* position to the phosphite unit.<sup>7</sup> Obviously, this effect is general also for acylphosphites with a smaller ring in the backbone. Interestingly, L4 allows also the achievement of a higher *n*-regioselectivity in the hydroformylation of *n*-octenes and 2-pentene. Unfortunately, inferior reaction rates resulted with L4, but this can be counteracted in a technical scale either by longer reaction times or by an increase of the temperature.

One of the most striking results of our study is that coordination to rhodium has different impacts on the hydrolysis stability of bidentate and monodentate ligands. The monodentate ligand L2 is stabilized in its Rh complex, while in strong contrast, the bidentate ligand L1 is faster hydrolyzed after coordination to Rh. In subsequent studies, it will be investigated whether this fact is general for monodentate and bidentate phosphites. This could have a strong influence on the applied Rh/ligand ratio of the hydroformylation in dependence on the type of the ligand used.

#### ■ ASSOCIATED CONTENT

##### Supporting Information

The Supporting Information is available free of charge on the ACS Publications website at DOI: 10.1021/acscatal.6b02185.

Preparation procedures, NMR spectra of hydrolysis experiments, hydroformylation details, X-ray crystallographic data, DFT calculation results (PDF)

Crystallographic data for L2 (CIF)

Crystallographic data for RhL2 (CIF)

Crystallographic data for L2DP4 (CIF)

Crystallographic data for L2-*t*Bu (CIF)

#### ■ AUTHOR INFORMATION

##### Corresponding Authors

\*E-mail: baixin.zhang@catalysis.de.

\*E-mail: armin.boerner@catalysis.de.

##### Notes

The authors declare no competing financial interest.

#### ■ ACKNOWLEDGMENTS

We acknowledge stimulating discussions with PD Dr. W. Baumann. We are thankful for the highly skilled technical assistance of Mrs. K. Romeike. We thank Dr. I. Otero for the preparation of some new phosphorus ligands. Financial support for this research was provided by Evonik Performance Materials GmbH.

#### ■ REFERENCES

- (1) *Homogeneous Catalysts, Activity – Stability – Deactivation*; van Leeuwen, P. W. N. M.; Chadwick, J. C., Eds.; Wiley-VCH: Weinheim, Germany, 2011; pp 227–231.
- (2) For some original literature, see the following: (a) Solinas, M.; Gladiali, S.; Marchetti, M. *J. Mol. Catal. A: Chem.* **2005**, 226, 141–147. (b) Abrams, M. L.; Foarta, F.; Landis, C. R. *J. Am. Chem. Soc.* **2014**, 136, 14583–14588. (c) Benetskiy, E.; Lüher, S.; Vilches-Herrera, M.; Selent, D.; Jiao, H.; Domke, L.; Dyballa, K.; Franke, R.; Börner, A. *ACS*



- Catal.* **2014**, *4*, 2130–2136. (d) Billig, E.; Abatjoglou, A. G.; Bryant, D. R.; Murray, R. E.; Mather, J. M. (to Union Carbide Corporation) U.S. Patent 4599206, 1986; U.S. Patent 4717775, 1988. (e) Billig, E.; Bryant, D. R. (to Union Carbide Chemicals & Plastics Technology Corporation) U.S. Patent 5767321, 1998.
- (3) (a) Bohnen, H.-W.; Cornils, B. *Adv. Catal.* **2002**, *47*, 1–64. (b) Wiese, K.-D.; Obst, D. In *Catalytic Carbonylation Reactions*; Beller, M., Ed.; Topics in Organometallic Chemistry **18**; Springer: Heidelberg, Germany, 2008; pp 1–33. (c) *Rhodium Catalyzed Hydroformylation*; van Leeuwen, P. W. N. M., Claver, C., Eds; Kluwer Academic Publishers: Dordrecht, Netherlands, 2000; p 16–22. (d) Franke, R.; Selent, D.; Börner, A. *Chem. Rev.* **2012**, *112*, 5675. Börner, A.; Franke, R. *Hydroformylation: Fundamentals, Processes, an Application in Organic Synthesis*; Wiley-VCH: Weinheim, Germany, 2016.
- (4) For examples, see the following: (a) Falbe, J. *New Synthesis with Carbon Monoxides*; Springer-Verlag: Berlin, Germany, 1980; p 158. (b) Blankertz, H.-J.; Grenacher, A. V.; Sauer, F.; Schwahn, H.; Schönmann, W. (to BASF Aktiengesellschaft) WO Patent 98/12235, 1998;. (c) Tötsch, W.; Arnoldi, D.; Kaizik, A.; Trocha, M. (to Oxeno Olefinchemie GmbH) WO Patent 03/078365, 2003;. (d) Canell, L. G.; Slaugh, L. H.; Mullineaux, R. D. (to Shell International Research Maatschappij B. V.) German Patent DE1186455, 1965;. (e) Drent, E.; Suykerbuyk, J. C. L. J. (to Shell International Research Maatschappij B. V.) WO Patent 2004054946, 2004.
- (5) For examples, see the following: (a) He, D.; Liu, J.; Liu, Y.; Wang, T.; Pang, D.; Chen, Y.; Liang, Y.; Zhu, Q. *Catal. Lett.* **2001**, *73*, 221. (b) Sato, K.; Miyazawa, C.; Wada, K.; Onoda, T. *Nippon Kagaku Kaishi* **1994**, 681. (c) He, D.; Pang, D.; Wang, T.; Chen, Y.; Liu, Y.; Liu, J.; Zhu, Q. *J. Mol. Catal. A: Chem.* **2001**, *174*, 21. (d) van Leeuwen, P. W. N. M.; Roobeek, C. F. *J. Organomet. Chem.* **1983**, *258*, 343. (e) van Rooy, A.; Orij, E. N.; Kamer, P. C. J.; van den Aardweg, F.; van Leeuwen, P. W. N. M. *J. Chem. Soc., Chem. Commun.* **1991**, 1096. (f) Jongsma, T.; Challa, G.; van Leeuwen, P. W. N. M. *J. Organomet. Chem.* **1991**, *421*, 121. (g) van Leeuwen, P. W. N. M.; Roobeek, C. (to Shell International Research Maatschappij B. V.) EP Patent 0054986, 1981;. (h) Abatjoglou, A. G.; Bryant, D. R.; Mather, J. M. (to Union Carbide Chemicals & Plastics Technology Corporation) EP Patent 0697391, 1995;. (i) Billig, E.; Abatjoglou, A. G.; Bryant, D. R. (to Union Carbide Corporation) EP Patent 213639, 1987; EP Patent 214622, 1987; U.S. Patent 4769498, 1988;. (j) Franke, R.; Borgmann, C.; Hess, D.; Wiese, K.-D. *Z. Anorg. Allg. Chem.* **2003**, *629*, 2535.
- (6) For a detailed discussion, see the following: (a) Janesko, B. G.; Fisher, H. C.; Bridle, M. J.; Montchamp, J.-L. *J. Org. Chem.* **2015**, *80*, 10025–10032. (b) Mehrotra, R. N. *Eur. Chem. Bull.* **2013**, *2*, 758–776. (c) Akbayeva, D. N.; Di Vaira, M.; Costantini, S. S.; Peruzzini, M.; Stoppioni, P. *Dalton Trans.* **2006**, 389–395.
- (7) Börner, A.; Franke, R. *Hydroformylation: Fundamentals, Processes, an Application in Organic Synthesis*; Wiley-VCH: Weinheim, Germany, 2016; pp 169–189.
- (8) Ueda, A.; Fujita, Y.; Kawasaki, H. (to Mitsubishi Chem. Corp. Japan), JP 2001342164, 2001; *Chem. Abstr.* **2001**, *136*, p 21214.
- (9) For some industrial approaches, see the following: (a) Dennis, A. J.; Harrison, G. E.; Wyber, J. P. (to Davy McKee (London) Limited) U.S. Patent 4567306, 1986;. (b) Hodan, J. J.; Schall, W.; Schall, W. L. (to Hooker Chemical Corporation) U.S. Patent 3553298, 1971;. (c) Billig, E.; Abatjoglou, G.; Bryant, D. R.; Murray, R. E.; Mather, J. M. (to Union Carbide Corporation) U.S. Patent 4599206, 1986; U.S. Patent 4717775, 1988;. (d) Babin, J. E.; Mather, J. M.; Billig, E. (to Union Carbide Chemicals & Plastics Technology Corporation) U.S. Patent 5364950, 1994;. (e) Abatjoglou, A. G.; Bryant, D. R.; Mather, J. M. (to Union Carbide Chemicals & Plastics Technology Corporation) U.S. Patent 5929289, 1999.
- (10) (a) Imaev, M. G.; Arbuzov, A. E. *Dokl. Akad. Nauk. SSSR* **1957**, *112*, 856. (b) Aksnes, G.; Aksnes, D. *Acta Chem. Scand.* **1964**, *18*, 1623–1628.
- (11) (a) McIntyre, S. K.; Alam, T. M. *Magn. Reson. Chem.* **2007**, *45*, 1022–1026. (b) Garland, M. C.; Pringle, P. G. *17th International Symposium on Homogeneous Catalysis*, Poznan, Poland, July 4–9, 2010; Abstract book p 158, poster p 82.
- (12) Janesko, B. G.; Fisher, H. C.; Bridle, M. J.; Montchamp, J.-L. *J. Org. Chem.* **2015**, *80*, 10025–10032.
- (13) Kraihanzel, C. S.; Bartish, C. M. *J. Am. Chem. Soc.* **1972**, *94*, 3572–3575. (b) Yakhvarov, D.; Caporali, M.; Gonsalvi, L.; Latypov, S.; Mirabello, V.; Rizvanov, I.; Sinyashin, O.; Stoppioni, P.; Peruzzini, M. *Angew. Chem., Int. Ed.* **2011**, *50*, 5370–5373. (c) Manca, G.; Caporali, M.; Ienco, A.; Peruzzini, M.; Mealli, C. *J. Organomet. Chem.* **2014**, *760*, 177–185.
- (14) For reviews, see the following: (a) Ackermann, L. *Synthesis* **2006**, No. 10, 1557–1571. (b) Ackermann, L. *Synlett* **2007**, 2007 (4), 0507–0526. (c) Ackermann, L.; Born, R.; Spatz, J. H.; Althammer, A.; Gschrei, C. *J. Pure Appl. Chem.* **2006**, *78*, 209–214. (d) Ackermann, L. In *Phosphorus Ligands in Asymmetric Catalysis*; Börner, A., Ed.; Wiley-VCH: Weinheim, Germany, 2008; Vols. I–III, pp 831–847. (e) Ackermann, L. *Pure Appl. Chem.* **2010**, *82*, 1403–1413.
- (15) For selected recent examples, see the following: (a) Bigeault, J.; de Riggi, I.; Gimbert, Y.; Giordano, L.; Buono, G. *Synlett* **2008**, 2008, 1071–1075. (b) Ackermann, L.; Potukuchi, H. K. *Synlett* **2009**, 2009, 2852–2856. (c) Ackermann, L.; Barfuesser, S. *Synlett* **2009**, 2009, 808–812. (d) Ackermann, L.; Potukuchi, H. K.; Althammer, A.; Born, R.; Mayer, P. *Org. Lett.* **2010**, *12*, 1004–1007. (e) Ackermann, L.; Wechsler, C.; Kapdi, A. R.; Althammer, A. *Synlett* **2010**, 2010, 294–298. (f) Ackermann, L.; Potukuchi, H. K.; Kapdi, A. R.; Schulzke, C. *Chem. - Eur. J.* **2010**, *16*, 3300–3303. Landert, H.; Spindler, F.; Wyss, A.; Blaser, H.-U.; Pugin, B.; Ribourduille, Y.; Gschwend, B.; Ramalingam, B.; Pfaltz, A. *Angew. Chem., Int. Ed.* **2010**, *49*, 6873–6876. (g) Achard, T.; Giordano, L.; Tenaglia, A.; Gimbert, Y.; Buono, G. *Organometallics* **2010**, *29*, 3936–3950.
- (16) (a) van Leeuwen, P. W. N. M.; Roobeek, C. F.; Wife, R. L.; Frijns, J. H. G. *J. Chem. Soc., Chem. Commun.* **1986**, 31–33. (b) van Leeuwen, P. W. N. M.; Roobeek, C. F.; Frijns, J. H. G.; Orpen, A. G. *Organometallics* **1990**, *9*, 1211–1222.
- (17) Dong, K.; Wang, Z.; Ding, K. *J. Am. Chem. Soc.* **2012**, *134*, 12474–12477.
- (18) Christiansen, A.; Selent, D.; Spannenberg, A.; Köckerling, M.; Reinke, H.; Baumann, W.; Jiao, H.; Franke, R.; Börner, A. *Chem. - Eur. J.* **2011**, *17*, 2120–2129.
- (19) Selent, D.; Hess, D.; Wiese, K.-D.; Röttger, D.; Kunze, C.; Börner, A. *Angew. Chem., Int. Ed.* **2001**, *40*, 1696–1698.
- (20) These downfield shifts are probably because of changes of intermolecular hydrogen bond interaction arising from the OH-group on the phosphorus atom.
- (21) (a) McIntyre, S. K.; Alam, T. M. *Magn. Reson. Chem.* **2007**, *45*, 1022–1026. (b) Westheimer, F. H.; Huang, S.; Covitz, F. *J. Am. Chem. Soc.* **1988**, *110*, 181–185.